Petroleum Research 11 (2026) 250–262

Contents lists available at ScienceDirect

Petroleum Research

journal homepage: http://www.keaipublishing.com/en/journals/petroleum-research/

Full Length Article

Mechanical analysis and structural optimization of anchorage for split segment inserted tooth slips

Zhongzhi Hu [a,*], Kaixin Lv [a], Xiang Gao [b], Zhilin Ye [b], Tiejun Lin [c]

[a] College of Mechanical Engineering, Sichuan University of Science and Engineering, Yibin, 644000, China
[b] Downhole Operation Research Department, CNPC Engineering Technology R&D Company Limited, Beijin, 102200, China
[c] State Key Laboratory of Oil and Gas Reservoir Geology and Exploitation, Southwest Petroleum University, Chengdu, 610000, China

ARTICLE INFO

Article history:
Received 15 February 2025
Received in revised form
3 August 2025
Accepted 3 August 2025
Available online 9 August 2025

Keywords:
Ultra-deep well
Packer
Slip
Anchoring
Mechanical behaviour

ABSTRACT

To meet the operational requirements of slip-type packers within TP140V casing in ultra-deep wells and enhance the anchoring performance and load-bearing capacity of the packer's anchoring mechanism during setting, this paper focuses on the study of tooth-embedded slips. The Abaqus finite element software was used to analyze the stress and contact pressure distribution patterns in key components such as the embedded teeth, casing, and slip base during the anchoring process of tooth-embedded slips. An orthogonal experimental method was employed to optimize the structural parameters of segmented tooth-embedded slips. Based on the results of the orthogonal experiments, the optimal combination of slip structural parameters was obtained: the front-end distance was 12 mm, the tooth installation spacing was 24 mm, the dip angle of the groove was 76.5°, the groove depth was 6.8 mm, and the slip wedge angle was 13°. After optimization, the maximum Von Mises stress in the slip base was reduced from 1080 MPa to 512.2 MPa, the embedding depth decreased from 0.2156 mm to 0.1338 mm, and the maximum contact pressure at the tooth tips dropped from 4247 MPa to 2965 MPa. Compared to the pre-optimization values, these reductions were 52.6%, 37.9%, and 30.2%, respectively. Moreover, the optimized casing bite depth and tooth-tip contact pressure exhibited a more uniform axial distribution. Additionally, physical prototypes of the optimized slips were manufactured and subjected to laboratory tests, which demonstrated that the axial bearing capacity of the slips could reach 450 kN, capable of withstanding axial loads in a 152.5-mm inner diameter casing under a downhole pressure environment of 100 MPa. The research findings in this paper provide a theoretical reference for optimizing the structural parameters of tooth-embedded slips within TP140V steel grade casing.

© 2025 Chinese Petroleum Society. Publishing services by Elsevier B.V. on behalf of KeAi Communications Co. Ltd. This is an open access article under the CC BY-NC-ND license (http://creativecommons.org/licenses/by-nc-nd/4.0/).

1. Introduction

As the exploitation of strata continues, oil and gas resources in China's middle and shallow strata are becoming increasingly scarce. The exploitation of deep and ultra-deep wells has become an important method for China to secure its oil and gas resources into the future (Ding et al., 2011; Su et al., 2020; Wang et al., 2022). In recent years, both the number of ultra-deep wells and well depth have continued to increase in China. Ultra-deep wells of over 8000 m have become normal, and 10 000-m deep wells are now being drilled. The deep-ground TK1 wells and deep-ground CK1 wells drilled by PetroChina in the Tarim Basin and Sichuan Basin in 2023 can serve as examples, as their designed vertical depths are 11 100 m and 10 520 m respectively (She, 2024; Sun et al., 2024; Wang et al., 2024). Geological conditions become more complex as well depth increases, and China has developed TP140V oil casing to meet the needs of ultra-deep well development (Chen et al., 2021; Lu et al., 2011; Tian et al., 2018). Slip packers achieve sealing and anchoring functions through the contact between the rubber barrel, slip, and casing. However, in deep and ultra-deep wells, the use of ultra-high-steel casing will cause the embedding of shallow slip teeth in the packer casing during setting, and unstable slip anchoring will lead to sealing failure (Cu et al., 2022; Hua and Qing, 2018; Yang et al., 2008; Zhao

* Corresponding author.
E-mail address: zhongzhi-hu@suse.edu.cn (Z. Hu).
Peer review under the responsibility of Editorial Office of Petroleum Research.

https://doi.org/10.1016/j.ptlrs.2025.08.002
2096-2495/© 2025 Chinese Petroleum Society. Publishing services by Elsevier B.V. on behalf of KeAi Communications Co. Ltd. This is an open access article under the CC BY-NC-ND license (http://creativecommons.org/licenses/by-nc-nd/4.0/).

et al., 2016). The slip is an important part of the packer, and the choice of material and structure design greatly influences its anchoring reliability. To meet the high anchor energy needs of higher steel-grade slips, materials with higher strength must be selected for their manufacture.

The slip structure can be divided into two types: milled and inserted (Deng, 2022). A milled slip is made of the whole material, and the substrate material strength of the inserted slip is low. When the embedded surface is hard, the choice is between greater hardness and higher-strength material machining teeth to improve the anchoring energy, and a smaller insert and lower-strength slip base costs less than whole-milling tooth slip processing. In addition, the insert slip structure greatly reduces the overall length of the setting tool, which is conducive to improving safety during construction (Wang et al., 2023).

In recent years, scholars have investigated various structural designs for inserted slips. Zhang et al. (2016) studied the influence of the main structural parameters of slips with inserts and milling teeth on anchor energy. Yu et al. (2013) summarized the law of the influence of the change of the axial angle of the timing slot of the insert slip anchor on the contact pressure of the inner wall of the casing. Wang et al. (2013) studied the influence of the tooth spacing of inserted slips on the setting safety of slips. Feng et al. (2017) analyzed the setting reliability of insert slips by studying the furrow shape formed after contact between slips with different insert teeth and casing as well as the displacement and stress between casing and insert teeth. Lu et al. (2022) established the physical balance relationship between slips and cones by analysing the timing stress of slip anchors. The same authors studied the influence law of the diameter of the mounting hole of slips and the angle of the slope cone of slips on the stress at the bottom of the mounting hole of the insert teeth. The results showed that changing the diameter of the hole and the angle of the slip's slope cone could improve the stress concentration at the bottom of the mounting hole of the insert teeth.

The above studies are based on the optimization and evaluation of the structural parameters of anchored and developed slips of steel grade, such as insert slips and P110. The applicability of higher-strength grades of casings still requires evaluation. Therefore, this paper takes insert slips as the research object. It adopts finite element numerical simulation and the orthogonal experimental analysis method to analyze the stress and strain law of insert slips and insert teeth during the anchoring process of insert slips and TP140V casing to complete the optimization of slip geometric parameters. The research results provide a certain reference value for the structural design and optimization of slips for internal packers with higher steel-grade casings.

2. Analysis of anchorage force on inserted slips

During the operation of the packer slip, the cone moves axially under the action of the setting load. When the wedge surface of the cone makes contact with the inclined surface of the slip base, the slip is pushed to move radially so that the slip insert is in contact with the casing. When the setting load is increased, the insert gradually bites into the inner wall of the casing to realize the positioning of the packer (Cui et al., 2023). The force analysis of the anchoring mechanism is simplified into the following components: cone, slip base, slip insert, and casing (see Fig. 1).

In Fig. 1, the upper end face of the cone is subject to axial force F; the wedge-shaped surface of the slip base is subject to the normal and tangential component forces R and f; and the horizontal and vertical component forces N and F_t are exerted by the casing on the insert teeth. According to the principle of static equilibrium, the force analysis of slips is obtained:

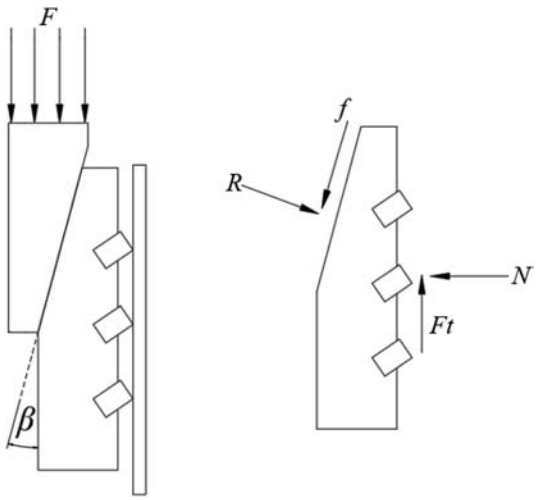


Fig. 1. Slip force analysis diagram.

$$F = R\sin\beta + f\cos\beta \tag{1}$$

Where: F is the axial force on the cone, kN; R is the normal component force on the single slip, kN; f is the tangential component force on the single slip, kN; and β is the cone angle of the slip base, °.

The relationship between the tangential component force f acting on the wedge face of the slip base and the friction coefficient is

$$f = \mu R \tag{2}$$

Where: μ is the friction coefficient between the slip and the casing.

$$\mu = \tan\varphi \tag{3}$$

Where: φ is the friction angle between the slip and the cone, °.

$$N = R\cos\beta - f\sin\beta \tag{4}$$

Where: N is the horizontal component force on a single slip, kN.

From formula (1) to formula (4), the horizontal component N of a single slip can be obtained as:

$$N = \frac{F}{\tan(\beta+\varphi)} \tag{5}$$

Fig. 2 is a diagram of the insert casing.

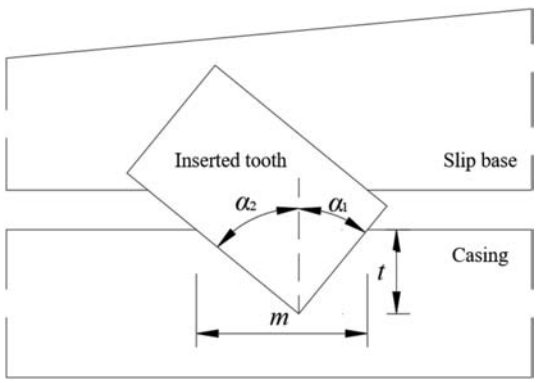


Fig. 2. Inserted tooth inserts casing diagram.

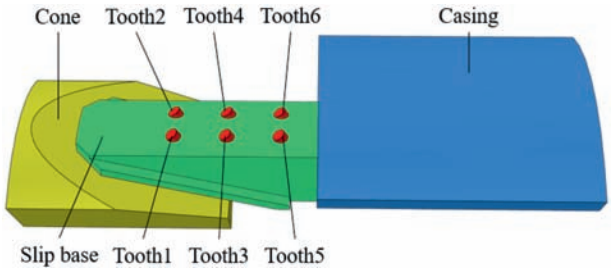


Fig. 3. Three-dimensional model of the inserted slip anchoring mechanism.

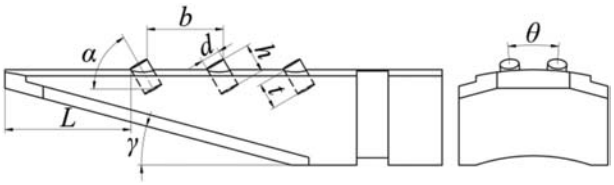


Fig. 4. Inserted slip structure diagram.

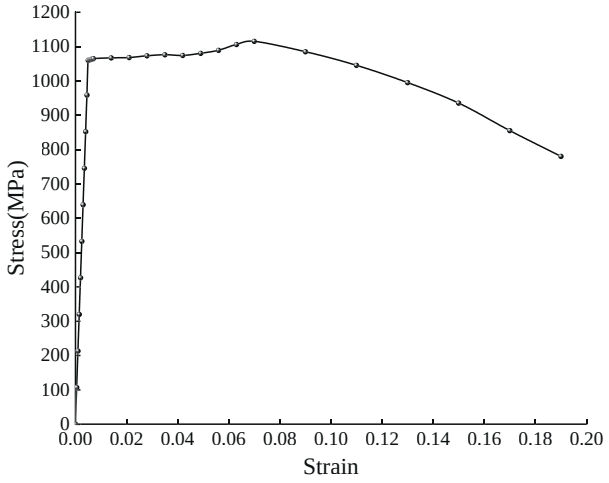


Fig. 5. Stress–strain curve of TP140V.

The following geometric relationship can be obtained from Fig. 2:

$$t=\frac{m}{\tan\alpha_1+\tan\alpha_2} \tag{6}$$

Where: t is the amount of casing insertion, mm; m is the length of casing insert, mm; α_1 is the front inclination of the tooth, °; and α_2 is the back inclination of the tooth, °.

The contact area S between the teeth and the casing is calculated approximately after the insert teeth are inserted into the casing:

$$S=\frac{\pi dm\phi}{360^\circ} \tag{7}$$

Where: φ is the contact angle between the insert circle and the casing, °; and d is the diameter of the upper round surface of the insert tooth, mm.

The contact stress σ between the slip insert and casing can be obtained by connecting the vertical (5) to formula (7):

$$\sigma=\frac{N}{S}=\frac{360^\circ F}{\pi dt\phi\tan(\beta+\varphi)(\tan\alpha_1+\tan\alpha_2)} \tag{8}$$

Where: σ is the contact stress between the slip insert and casing, MPa.

3. Slip-anchoring finite element model

3.1. Finite element model building

The inserted slip-anchoring mechanism is composed of six pieces of slip base symmetrically. To improve the efficiency of numerical simulation to ensure accurate calculations, one-sixth of the whole mechanism is taken for anchoring energy analysis. The three-dimensional model is shown in Fig. 3. In Fig. 3, the casing diameter is 177.8 mm, the wall thickness is 12.65 mm, and the insert teeth are numbered from 1 to 6; the cylindrical edge of the upper end of the insert teeth is filleted, and the curvature radius is 0.2 mm (Han et al., 2020). The structure parameters of the inserted slips are shown in Fig. 4.

As shown in Fig. 4, the key parameters of the insert-tooth slip structure primarily include the tooth end distance L, the tooth spacing b, the tooth groove angle α, the tooth groove depth t, the slip cone angle γ, the tooth diameter d, the tooth height h, and the circumferential angle θ. Based on the structural parameter values or approximate references from the related insert-tooth slip literature (Hao et al., 2019; Wang et al., 2021; Liu, 2023), combined with casing/tubing dimensions, circumferential slip arrangement, and practical engineering requirements, the structural parameters of the slip designed in this study are preliminarily determined as follows: $L = 25$ mm, $b = 27$ mm, $\alpha = 75°$, $t = 6.5$ mm, $\gamma = 10°$, $d = 8$ mm, $h = 8.5$ mm, and $\theta = 12°$.

3.2. Material parameter setting

The casing material selected in this study is TP140V steel. To accurately characterize the deformation behaviour during

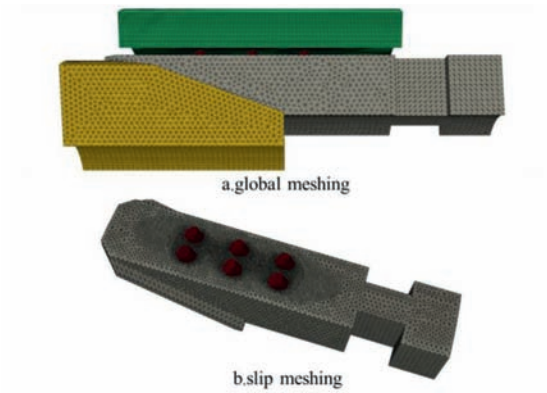


Fig. 6. Meshing.

Table 1
Mechanical property parameters of materials.

Component	Young's modulus/MPa	Poisson'ratio	Yield stress/MPa	Tensile strength/MPa
Cone、Slip base	2.10×10^5	0.26	1080	1175
Tooth	6.40×10^5	0.22	5460	–
Casing	2.13×10^5	0.29	1065	1115

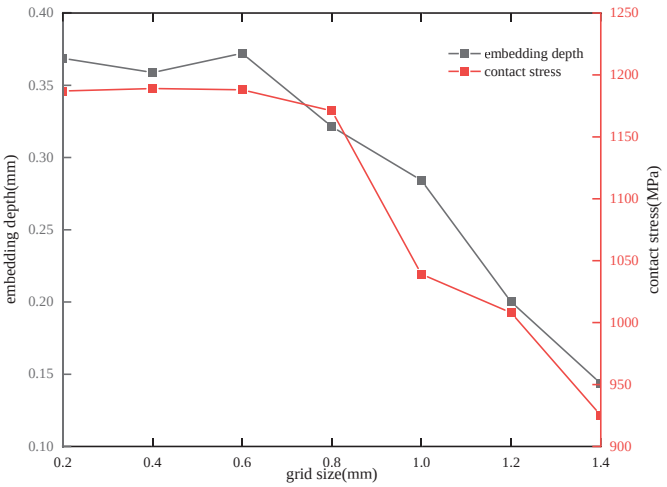


Fig. 7. Contact position grid independence verification.

casing–slip teeth contact, uniaxial tensile tests were conducted in accordance with GB/T 228-2002 (Tensile Test Method for Metal Materials at Room Temperature). The obtained stress–strain curve of the casing material is shown in Fig. 5. The measured material parameters include elastic modulus $E = 213$ GPa, Poisson's ratio $\mu = 0.3$, yield strength $\sigma_y = 1065$ MPa, and ultimate tensile strength $\sigma_b = 1115$ MPa. Given the approximately linear characteristics of the material's plastic hardening stage, a bilinear model was adopted in the numerical simulation software to describe the plastic deformation of the casing.

The cone and slip base are fabricated from high-strength alloy steel 20Cr2Ni4 (Pang et al., 2015), modelled using an ideal elastoplastic constitutive relationship. Insert teeth, which are critical in ensuring packer setting stability and service performance during installation and operation, require high hardness, superior strength, impact resistance, structural stability, and high-temperature endurance under ultra-deep well conditions. Current industry standards predominantly employ cemented carbide materials for such applications (Xu, 2011). ZD10U cemented carbide was selected as the insert material, with yield strength adopted as the failure criterion to ensure adequate safety margins. The key material properties of components are summarized in Table 1.

3.3. Meshing

A finite element model for the insert-tooth slip and perform meshing was established with the mesh division shown in Fig. 6. Considering the irregular geometries of the slip base and cone, C3D4 (a 4-node linear tetrahedral element) was selected as the element type, with local mesh refinement implemented at the

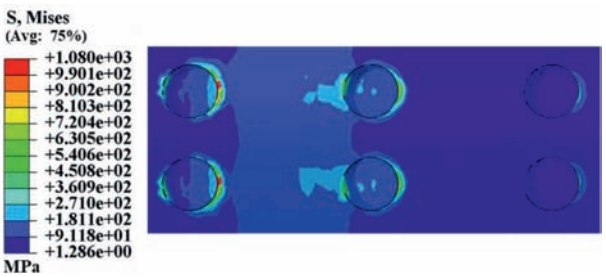


Fig. 8. Stress nephogram of slip base.

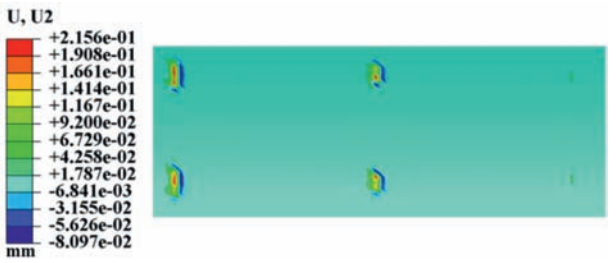


Fig. 9. Tooth marks distribution nephogram.

tooth–hole contact areas. For regularly shaped components (insert teeth and casing), the sweep meshing technique was adopted using the C3D8R (8-node hexahedral linear reduced integration element) as the element type.

As the contact parts of the insert-casing and insert-slip base are the main analysis objects, only the grid refinement degree of the contact area was changed during the grid independence verification. The grid independence verification results are shown in Fig. 7. As can be seen from Fig. 7, when the grid size is lower than 0.6 mm, the sensitivity of the calculated results to the grid density gradually eases, and the embedding depth increases from 0.3588 mm to 0.3687 mm, with a change of less than 3%. The casing contact stress increases from 1187 MPa to 1189 MPa, and the change does not exceed 1%. Therefore, considering the calculation efficiency and accuracy comprehensively, a grid of 0.4 mm was selected for subsequent simulation calculations.

3.4. Load, boundary condition setting

(1) During cementing, the outer wall of the casing was fixed by cement, the fixed constraint was applied to the outer wall of the casing. (2) The slip circumference was evenly distributed; one of the six slips was analyzed, the cone thrust was set according to 1/6, and the axial setting load of 25 kN was applied. (3) When working, the slip moves radially under the action of the cone extrusion to achieve anchoring. Therefore, the degree of freedom—other than the radial direction of the lower end face of the slip base—is limited, and binding constraints were adopted for the slip base and insert teeth. (4) Since the materials of each component are steel, the friction coefficient at each contact point of the model was set to 0.15 (Hao et al., 2019).

3.5. Results of finite element calculation of slip setting under initial conditions

The stress distribution of the slip base is shown in Fig. 8. As can be seen from the cloud image of the slip base in Fig. 8, the maximum equivalent stress of the slip base ranges from 990.1 MPa to 1080 MPa, reaching the yield strength of 20Cr2Ni4 of the base material. The maximum stress value is mainly concentrated at the

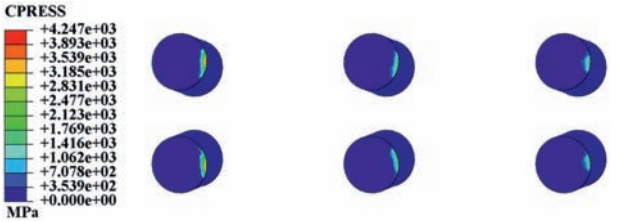


Fig. 10. Tooth tip contact pressure distribution nephogram.

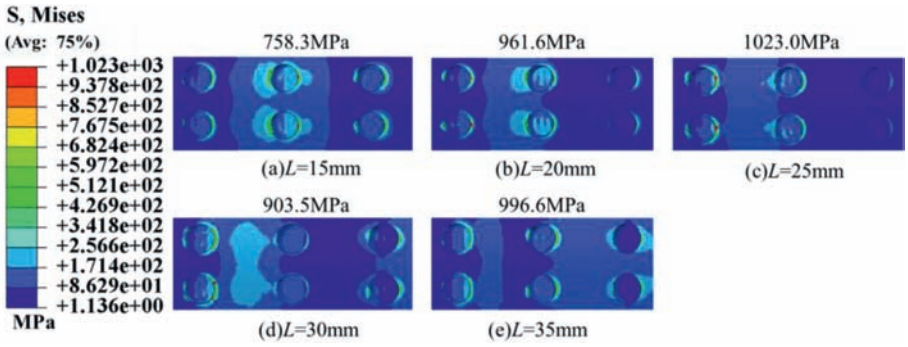


Fig. 11. Stress nephogram of slip base under different front-end distances.

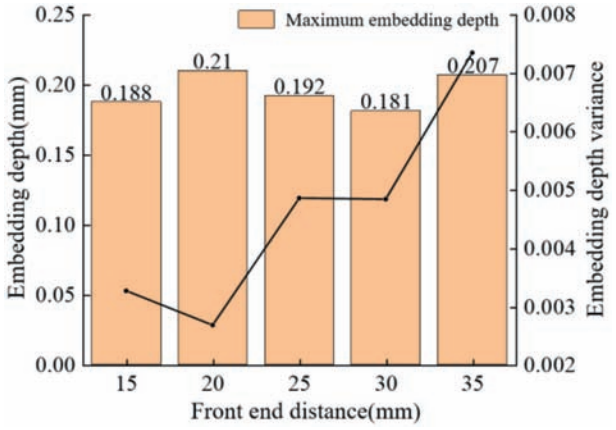


Fig. 12. Maximum embedding depth and embedding depth variance of casing under different front-end distances.

edge of the tooth groove, indicating that the matrix has undergone plastic deformation after the anchoring of the slip and that damage has occurred around the tooth groove. The tooth marks on the inner wall of the casing and the pressure distribution of the insert tooth tip after the slip anchoring are shown in Figs. 9 and 10. As shown in the cloud map of tooth mark distribution and contact pressure distribution of the tooth tip in Figs. 9 and 10, there is uneven occlusion between the teeth and the casing in the process of slip anchoring casing, which will reduce the stability of the slip anchoring.

Based on the comprehensive analysis above, it is evident that the insert-tooth slip anchor is prone to tooth slot damage and non-uniform tooth engagement during anchoring. Therefore, this paper first conducted a single-factor influence test on the front tooth end distance, tooth spacing, tooth slot inclination, tooth groove depth, and slip cone angle to explore the influence law of tooth layout and slip structure on the stress of slip base, tooth mark depth, and tooth occlusion uniformity. Then, an orthogonal test was carried out to determine the optimal design of slip structure parameters, and the reliability of the research results was tested and verified.

4. Analysis of the influence of tooth layout and slip structure parameters on the force of the slip base

4.1. Front-end distance

Setting the front end distance L = 15 mm, 20 mm, 25 mm, 30 mm, and 35 mm respectively, the stress value of the slip base, the maximum embedding depth of casing U_{max}, and the

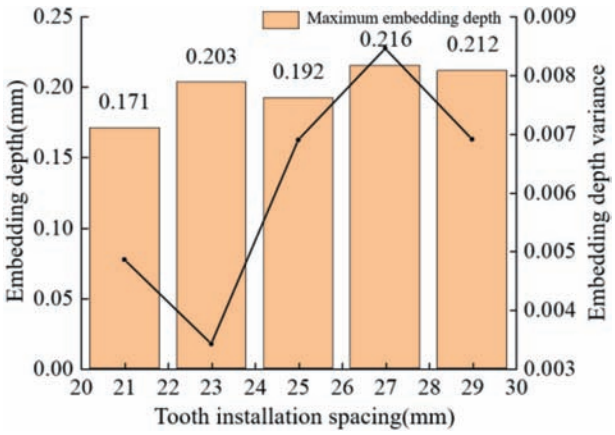


Fig. 14. Maximum embedding depth and embedding depth variance of casing under different tooth installation spacings.

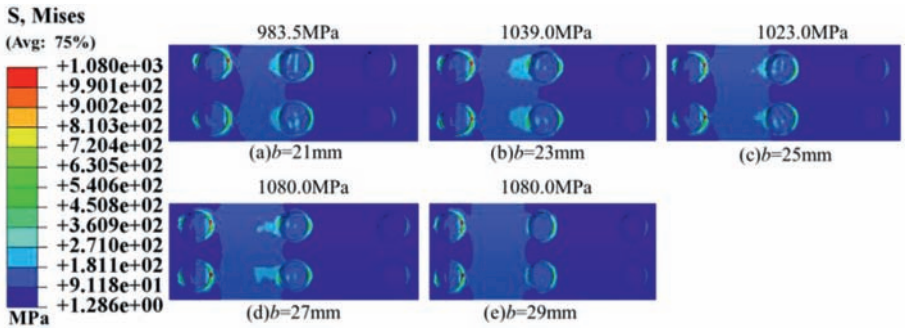


Fig. 13. Stress nephogram of slip base under different tooth installation spacings.

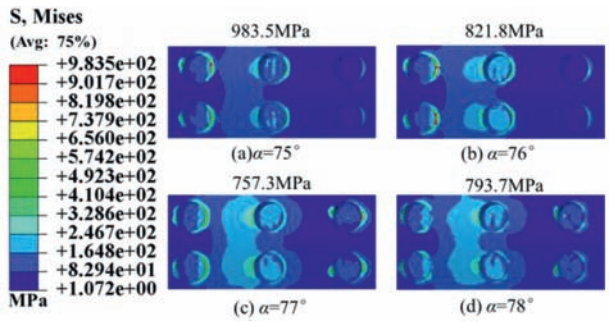


Fig. 15. Stress nephogram of slip base under different dip angles of groove.

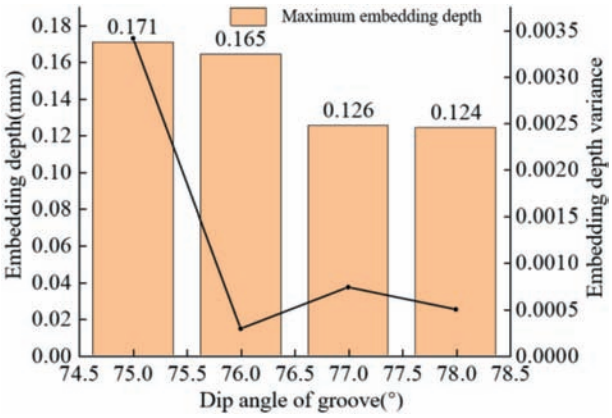


Fig. 16. Maximum embedding depth and embedding depth variance of casing under different dip angles of grooves.

embedding depth variance of the casing are respectively set as shown in Figs. 11 and 12. It can be seen from Figs. 11 and 12 that the change of tooth end distance has little influence on the casing embedding depth, and the maximum stress of the slip base does not exceed the yield strength of the material. When L = 15 mm and 20 mm, the embedding depth variance is small, and the teeth bite more evenly.

4.2. Tooth installation spacing

Setting the tooth installation spacing b = 21 mm, 23 mm, 25 mm, 27 mm, and 29 mm, respectively, the stress value of the slip base, the maximum embedding depth of casing U_{max}, and the embedding depth variance of casing are shown in Figs. 13 and 14. As can be seen from Figs. 13 and 14, the stress value of the slip base shows an overall increasing trend with the increase of tooth installation spacing. When tooth spacing b = 27 mm and 29 mm, the stress of the slip base reaches the yield strength of the material, resulting in plastic deformation.

4.3. Dip angle of groove

Setting the dip angle of the groove α = 75°, 76°, 77°, and 78°, respectively, and comparing the stress of the slip base, the maximum embedding depth of casing U_{max} and the embedding depth variance of casing are shown in Figs. 15 and 16. It can be seen from Figs. 15 and 16 that the stress value of the slip base and the maximum embedding depth of the casing tend to decrease overall with the increase of the dip angle of the groove. When α = 75°, the embedding depth variance is large, and the uneven phenomenon of the casing anchored by the slip is obvious.

4.4. Groove depth

Setting the groove depth t = 6.3 mm, 6.4 mm, 6.5 mm, 6.6 mm, and 6.7 mm, respectively, the stress value of the slip base, the maximum embedding depth of casing U_{max}, and the embedding depth variance of casing are shown in Figs. 17 and 18. It can be seen from Figs. 17 and 18 that the stress value of the slip base is largest when the groove depth t = 6.4 mm, and the embedding depth is the deepest when t = 6.3 mm.

4.5. Slip wedge angle

Setting the slip wedge angle γ = 10°, 12°, and 14°, respectively, and comparing the stress of the slip base, the maximum

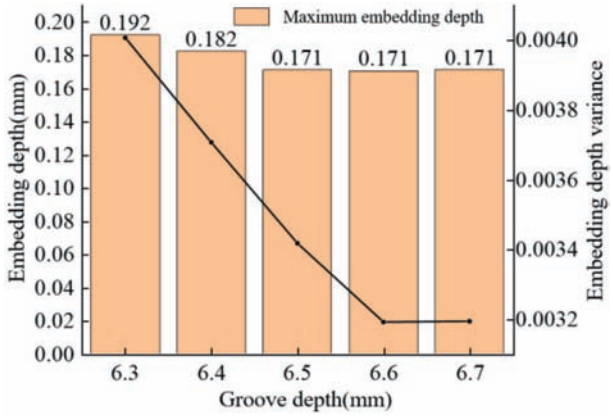


Fig. 18. Maximum embedding depth and embedding depth variance of casing under different groove depths.

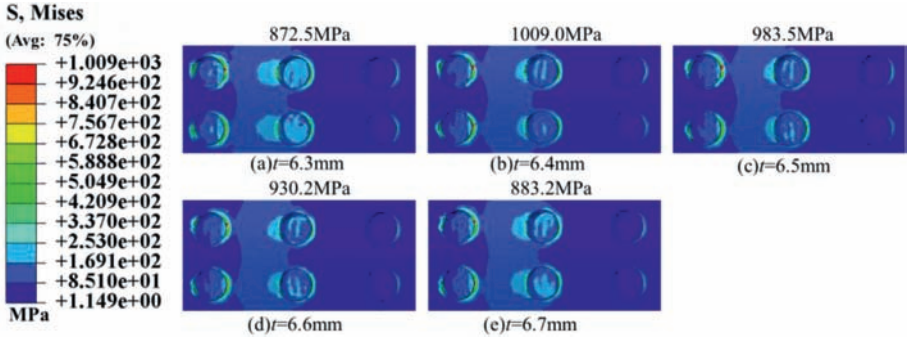


Fig. 17. Stress nephogram of slip base under different groove depths.

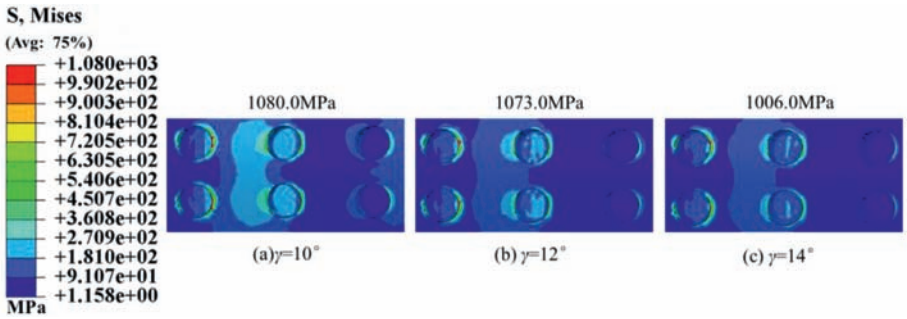


Fig. 19. Stress nephogram of slip base under different slip wedge angles.

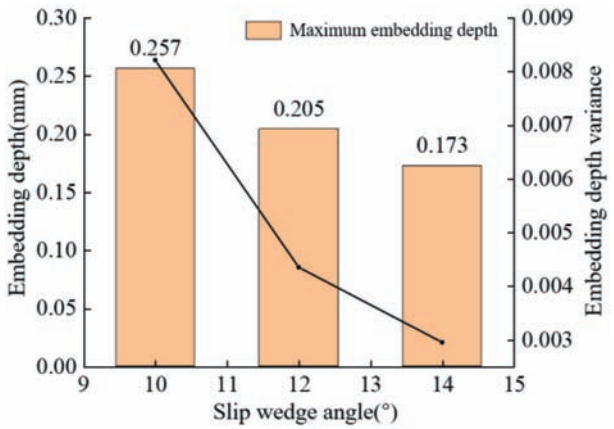


Fig. 20. Maximum embedding depth and embedding depth variance of casing under different slip wedge angles.

embedding depth of casing U_{max} and the embedding depth variance of casing are shown in Figs. 19 and 20. It can be seen from Figs. 19 and 20 that when the slip wedge angle $\gamma = 10$ mm and 12 mm, the maximum stress of the slip base is close to the yield strength of the material, and when $\gamma = 14$ mm, the maximum embedding depth of the casing and the embedding depth variance of the casing are smallest.

5. Orthogonal experiment optimization and test verification

5.1. Orthogonal test

To optimize the slip structure parameters, the orthogonal test method was used in this paper to obtain reliable experimental results with fewer experimental trials. The evaluation indices of the test are as follows: the minimum stress of the slip base, the minimum embedding depth, and the minimum variance. The level table of test factors is shown in Table 2. The 16 groups of structural parameters shown in Table 3 were constructed using combinatorial mathematical theory, and the corresponding results were obtained through finite element simulation.

(1) Intuitive analysis

According to the test results obtained in Table 3, the curve shown in Fig. 21 can be obtained. From Fig. 21, it can be intuitively seen that scheme 15 is the optimal combination ($L_4b_3\alpha_2t_4\gamma_1$) when the stress of the slip base is the main evaluation standard. When the maximum embedding depth was the main evaluation criterion, scheme 9 was the optimal combination ($L_3b_1\alpha_3t_4\gamma_2$). Scheme 15 was the optimal combination ($L_4b_3\alpha_2t_4\gamma_1$) when variance was the main evaluation criterion.

(2) Range analysis

The degree of influence of the selected level of each factor on the test results can be obtained through range analysis. The greater the range value, the greater the influence of the selected level of the factor on the test results. According to the calculations of formulas (9) and (10), the influence of each factor level on the three test indicators is extremely poor, and the results are shown in Tables 4–6.

$$\begin{cases} \overline{K_i} = \dfrac{\sum A}{m} \\ \overline{K_i'} = \dfrac{\sum B}{m} \\ \overline{K_i''} = \dfrac{\sum C}{m} \end{cases} \tag{9}$$

$$\begin{cases} R = Max\overline{K_i} - Min\overline{K_i} \\ R' = Max\overline{K_i'} - Min\overline{K_i'} \\ R'' = Max\overline{K_i''} - Min\overline{K_i''} \end{cases} \tag{10}$$

Where: i is the number of levels, $i = 1$–4; m is the number of levels of factors in each column, $m = 4$; A, B, and C are the corresponding test data values of the result items.

Table 2
Structure optimization factor level table.

Level	Influencing factor				
	Front end distance L/mm	Tooth installation space b/mm	Dip angle of groove α/(°)	Groove depth t/mm	Slip wedge angle γ/(°)
1	19	21	76.0	6.5	13.0
2	20	22	76.5	6.6	13.5
3	21	23	77.0	6.7	14.0
4	22	24	77.5	6.8	14.5

Table 3
Orthogonal experiment scheme and results.

Scheme	Factor					Result		
	Front end distance L/mm	Tooth installation space b /mm	Dip angle of groove α/(°)	Groove depth t/mm	Slip wedge angle γ/(°)	Slip base stress A/MPa	Embedding depth B/mm	Variance C
1	19	21	76.0	6.5	13.0	1007.0	0.17	1.45×10^{-3}
2	19	22	76.5	6.6	13.5	925.1	0.17	0.55×10^{-3}
3	19	23	77.0	6.7	14.0	728.3	0.18	2.39×10^{-3}
4	19	24	77.5	6.8	14.5	837.7	0.13	0.71×10^{-3}
5	20	21	76.5	6.7	14.5	799.5	0.14	1.42×10^{-3}
6	20	22	76.0	6.8	14.0	749.3	0.14	0.83×10^{-3}
7	20	23	77.5	6.5	13.5	821.1	0.18	3.11×10^{-3}
8	20	24	77.0	6.6	13.0	745.5	0.14	0.98×10^{-3}
9	21	21	77.0	6.8	13.5	706.7	0.11	0.41×10^{-3}
10	21	22	77.5	6.7	13.0	870.4	0.15	1.56×10^{-3}
11	21	23	76.0	6.6	14.5	814.0	0.16	1.01×10^{-3}
12	21	24	76.5	6.5	14.0	717.1	0.12	0.81×10^{-3}
13	22	21	77.5	6.6	14.0	768.4	0.14	0.65×10^{-3}
14	22	22	77.0	6.5	14.5	776.8	0.15	1.69×10^{-3}
15	22	23	76.5	6.8	13.0	471.8	0.12	0.25×10^{-3}
16	22	24	76.0	6.7	13.5	598.0	0.13	0.89×10^{-3}

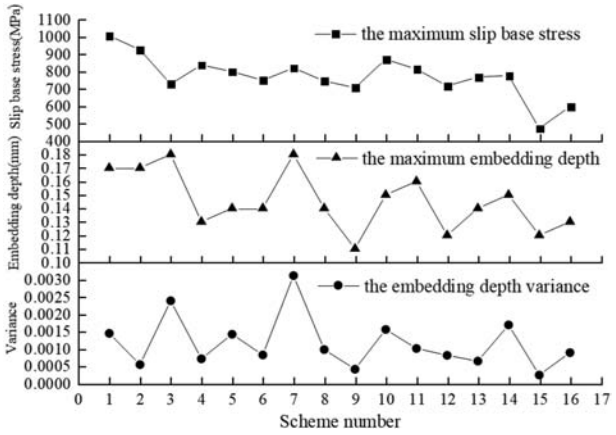


Fig. 21. Orthogonal test results curve.

According to the range values in Table 4, the influence of the five factors on the maximum stress of the slip base is as follows: front-end distance > groove depth > tooth installation space > dip angle of groove > slip wedge angle. According to the range values in Table 4, the influence of the five factors on the maximum stress of the slip base is as follows: groove depth = tooth installation space > front-end distance > dip angle of groove > slip wedge angle.

From the range values in Tables 6, it can be seen that the influence of the five factors on the uniformity of the embedding depth of each tooth is in descending order: groove depth > tooth installation space > dip angle of groove > front-end distance > slip wedge angle. To intuitively see the impact of the changes of various factors on the test results, the relationship curves between factor levels and indicators are drawn in Figs. 22–24, taking the level of factors as the horizontal coordinate and the average value in Tables 4–6 as the vertical coordinate. As can be seen from Fig. 22, $L_4b_3\alpha_2t_4\gamma_3$ is the optimal scheme that takes the maximum stress of the slip base as the evaluation index. As can be seen from Fig. 23, the optimal scheme using the maximum embedding depth as the evaluation index is $L_3b_4\alpha_2t_4\gamma_1$, $L_3b_4\alpha_2t_4\gamma_3$, $L_3b_4\alpha_2t_4\gamma_4$, $L_4b_4\alpha_2t_4\gamma_1$, $L_4b_4\alpha_2t_4\gamma_3$, $L_4b_4\alpha_2t_4\gamma_4$. As can be seen from Fig. 24, $L_4b_4\alpha_2t_4\gamma_1$ is the optimal scheme for evaluating the uniformity of the inserted casing with each tooth.

Based on the above intuitive analysis and range analysis, the following ten optimal schemes are obtained: $L_4b_3\alpha_2t_4\gamma_1$, $L_3b_1\alpha_3t_4\gamma_2$, $L_4b_3\alpha_2t_4\gamma_1$, $L_4b_4\alpha_2t_4\gamma_3$, $L_3b_4\alpha_2t_4\gamma_3$, $L_3b_4\alpha_2t_4\gamma_4$, $L_4b_4\alpha_2t_4\gamma_1$, $L_4b_4\alpha_2t_4\gamma_3$, $L_4B_4\alpha_2t_4\gamma_4$, $L_4B_4\alpha_2t_4\gamma_3$, $L_4B_4\alpha_2t_4\gamma_4$. The results of the occurrence times of each level in the statistical factors are shown in Table 7. According to Tables 7, in 10 schemes, the frequency of the fourth level of front-end distance L is 6/10, the fourth level of tooth installation distance b is 6/10, the second level of dip angle of groove α is 9/10, the fourth level of groove depth t is 10/10, and the first level of slip wedge angle is 4/10. Therefore, the optimal slip structural parameter scheme is $L_4b_4\alpha_2t_4\gamma_1$, and the corresponding slip structural parameters are as follows: front-end distance $L = 12$ mm, tooth installation space $b = 24$ mm, slip angle of groove $\alpha = 76.5°$, groove depth $t = 6.8$ mm, and slip wedge angle $\gamma = 13°$.

(3) Optimization results of orthogonal experiments

The combined simulation analysis of the optimized parameters was carried out, and the distribution of slip base stress, tooth mark, and contact stress is shown in Fig. 25. Compared with the simulation results before optimization, it can be concluded that the maximum stress of the slip base, the maximum embedding depth, and the maximum contact stress are lower after optimization. The stress of the slip base is reduced by 52.6%, the maximum depth is reduced by 37.9%, and the maximum contact stress is reduced by

Table 4
Maximum slip base stress range analysis.

	Average value	Front end distance L/mm	Tooth installation space b/mm	Dip angle of groove α/(°)	Groove depth t/mm	Slip wedge angle γ/(°)
Slip base stress	$\overline{K_1}$	874.5250	820.4000	792.0750	830.5000	773.6750
	$\overline{K_2}$	778.8500	830.4000	728.3750	813.2500	762.7250
	$\overline{K_3}$	777.0500	708.8000	739.3250	749.0500	740.7750
	$\overline{K_4}$	653.7500	724.5750	824.4000	691.3750	807.0000
Range value		220.7750	121.6000	96.0250	139.1250	66.2250

Table 5
Maximum embedding depth range analysis.

	Average value	Front end distance L/mm	Tooth installation space b/mm	Dip angle of groove α/(°)	Groove depth t/mm	Slip wedge angle γ/(°)
Embedding depth	$\overline{K_1'}$	0.1625	0.1400	0.1500	0.1550	0.1450
	$\overline{K_2'}$	0.1500	0.1525	0.1375	0.1525	0.1475
	$\overline{K_3'}$	0.1350	0.1600	0.1450	0.1500	0.1450
	$\overline{K_4'}$	0.1350	0.1300	0.1500	0.1250	0.1450
Range value		0.0275	0.0300	0.0125	0.0300	0.0025

Table 6
Analysis of uniformity of embedment depth of each tooth.

	Average value	Front end distance L/mm	Tooth installation space b/mm	Dip angle of groove α/(°)	Groove depth t/mm	Slip wedge angle γ/(°)
Variance	$\overline{K_1''}$	1.27×10^{-3}	0.98×10^{-3}	1.04×10^{-3}	1.77×10^{-3}	1.06×10^{-3}
	$\overline{K_2''}$	1.59×10^{-3}	1.16×10^{-3}	0.76×10^{-3}	0.80×10^{-3}	1.24×10^{-3}
	$\overline{K_3''}$	0.95×10^{-3}	1.69×10^{-3}	1.37×10^{-3}	1.57×10^{-3}	1.17×10^{-3}
	$\overline{K_4''}$	0.87×10^{-3}	0.85×10^{-3}	1.51×10^{-3}	0.55×10^{-3}	1.21×10^{-3}
Range value		0.72×10^{-3}	0.84×10^{-3}	0.75×10^{-3}	1.22×10^{-3}	0.18×10^{-3}

30.2%. The distribution of embedding depth and contact stress before and after optimization is shown in Fig. 26. It can be seen from Fig. 26 that the contact stress between each tooth and casing and the embedding depth are more evenly distributed than before optimization, which indicates that the anchorage quality between the inserted tooth slip and casing is improved after improving the parameters.

5.2. Laboratory test verification

To verify the science and feasibility of the design, the corresponding slips were processed according to the optimization results, and the slip anchoring test in TP140V steel casing was carried out in the packer slip setting test system of CNPC Engineering Technology R&D Company Limited. The test equipment, prototype, and principle are shown in Fig. 27. The test reference standard was SY/T 5049-2009.

(1) Experimental design and process

There are three pairs of slips in the packer. In this test, one pair of slips was selected for circumferentially symmetrical distribution to test performance. The load is set at 1/3 in both setting and bearing tests. First, the setting load of 50 kN was

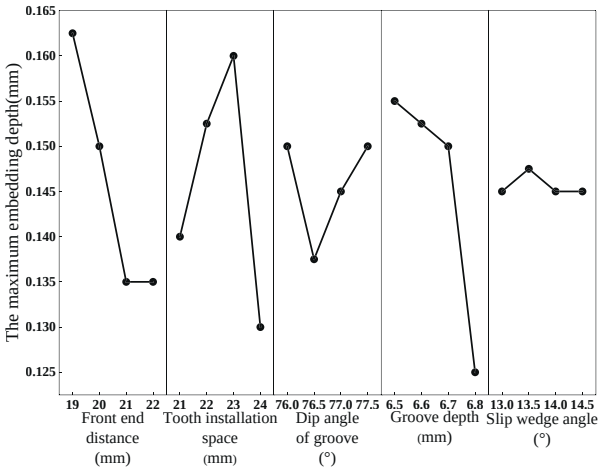


Fig. 23. Maximum embedded depth index vs. factor level.

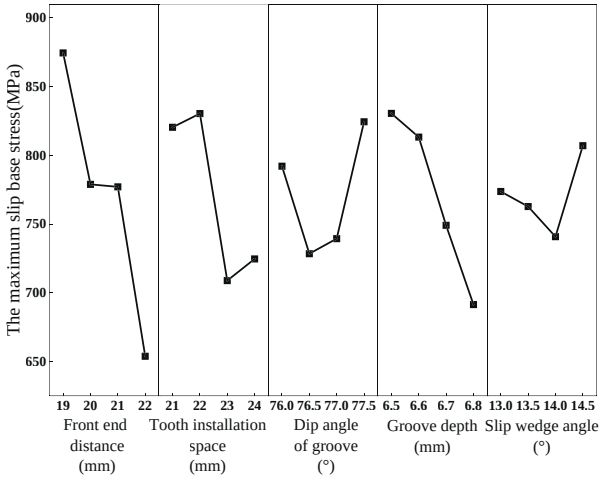


Fig. 22. Maximum stress of slip base index vs. factor level.

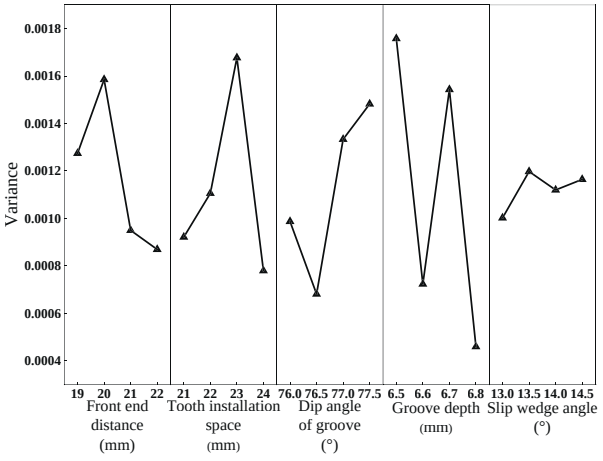


Fig. 24. The embedded depth variance index vs. factor level.

Table 7
The occurrence times of different levels of each factor.

Factor level	Front end distance L/mm	Tooth installation space b/mm	Dip angle of groove α/(°)	Groove depth t/mm	Slip wedge angle γ/(°)
First level	0	1	0	0	4
Second level	0	0	9	0	1
Third level	4	3	1	0	3
Forth level	6	6	0	10	2

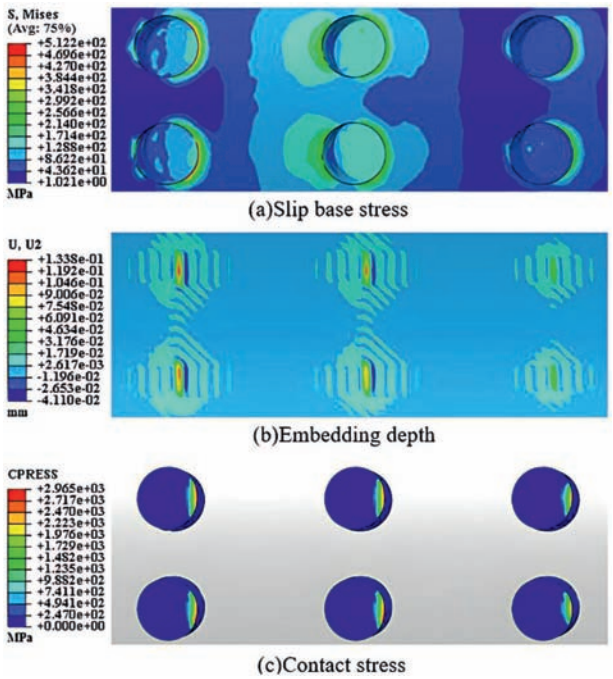


Fig. 25. Nephogram of slip base stress, embedded depth of casing, and tooth tip contact pressure.

applied to the small piston end, and the tooth mark depth of the casing wall was measured to verify the simulation results. Then, the load Qa was applied from the big piston cylinder, and the change of slip displacement and force loading was observed to determine the bearing capacity of the slip.

Setting test: press to 50 kN through port A, push the slip seat through the right end of the small piston push rod to stabilize the pressure for 2 min after the slip is set and the anchor casing is fixed; then, the small piston cylinder is relieved and reset, and the depth of each tooth mark on the inner wall of the casing is measured by removing the slip and compared with the simulation results.

Bearing test: apply a relatively small setting load from port A such that the slip teeth make initial contact with the casing wall, and close port A. Press down to 50 kN from port B to further bite the slip teeth into the casing; then, open the pressure relief valve at port A, and continue to press from port B to judge the anchorage of the slip by observing the change of load and displacement value. If the load value does not rise and the displacement changes, repeat the previous steps until the load value can be stabilized at a certain value for 5 min without a displacement change.

(2) Analysis of test results

Figs. 28 and 29 show the comparison diagram of tooth mark distribution in 140 steel grade casing under a 50 kN setting load and the comparison curve diagram of tooth mark depths between the simulation and test. Comparative analysis of Figs. 28 and 29 demonstrates a close alignment between the numerical simulations and experimental results, validating the reliability of the computational model. As shown in Fig. 28, the optimized slips exhibit a uniform axial penetration depth distribution of the front/rear teeth during casing contact, achieving the orthogonal optimization objectives.

Fig. 30 presents the load-bearing performance test curves of the optimized slip configuration. It can be seen from Fig. 30 that when the load reaches the peak value of 200 kN, it drops suddenly and then becomes 0 instantly. The displacement also decreases by 5 mm and then drops to 0, which indicates that slip occurs at this time, and the slip cannot continue to anchor the casing, thus losing the bearing capacity. When the load value is 150 kN, the stability time is 5 min, which represents the stable bearing capacity of the slip. That is, the bearing capacity of the packer can be up to 450 kN in practical application. To verify whether the bearing capacity of

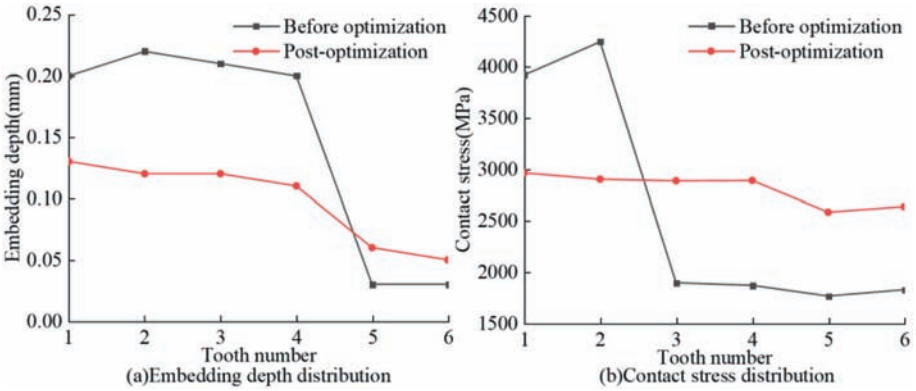


Fig. 26. The distribution of embedding depth and contact stress before and after optimization.

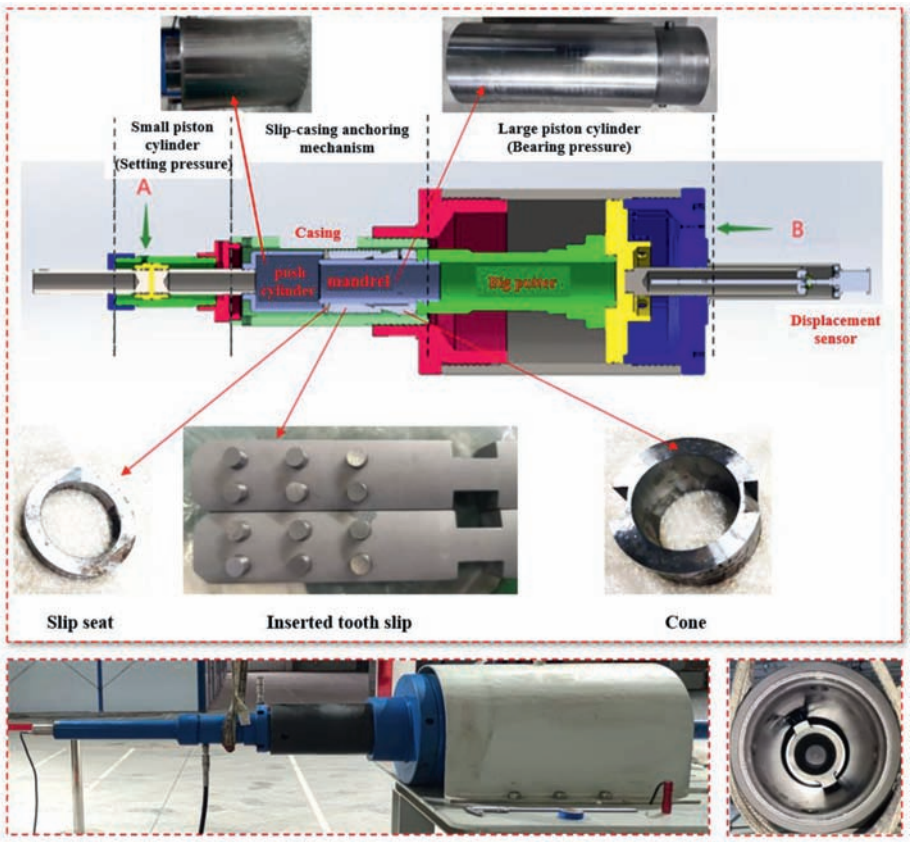


Fig. 27. Packer slip setting test device.

the slip meets the requirements, force analysis was carried out on the packer, and the setting diagram is shown in Fig. 31.

It can be seen from Fig. 31 that a pressure difference is generated by different upper and lower pressure areas during the packer setting. Assuming that all the pressure difference is borne by slips, the working pressure difference F_z required by slips under 100 MPa condition can be obtained by connecting vertical lines (9) and equation (10).

$$\begin{cases} A_1 = \dfrac{\pi}{4}\left(d_f^2 - d_0^2\right) \\ A_2 = \dfrac{\pi}{4}\left(d_f^2 - d_1^2\right) \end{cases} \tag{9}$$

$$F_z = P(A_1 - A_2) \tag{10}$$

Where: A_1 is the pressure area at the lower end of the packer, mm^2; A_2 is the upper pressure area of the packer, mm^2; d_f is the outer

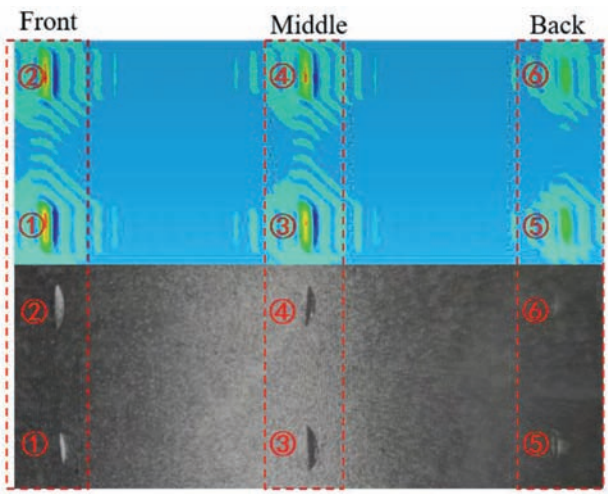


Fig. 28. Distribution of casing tooth marks after slip anchoring.

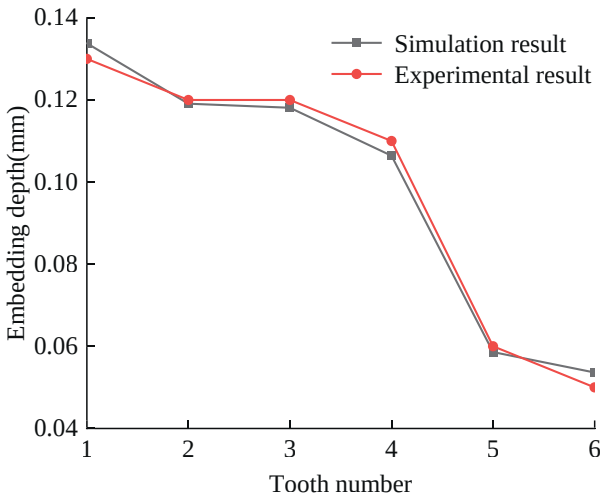


Fig. 29. Comparison of theoretical and experimental embedding depths.

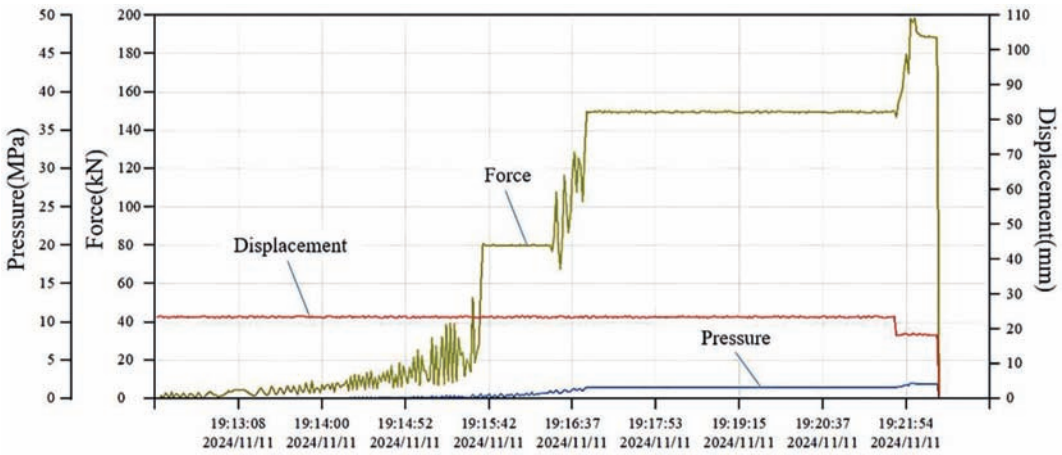


Fig. 30. Slip bearing test curve.

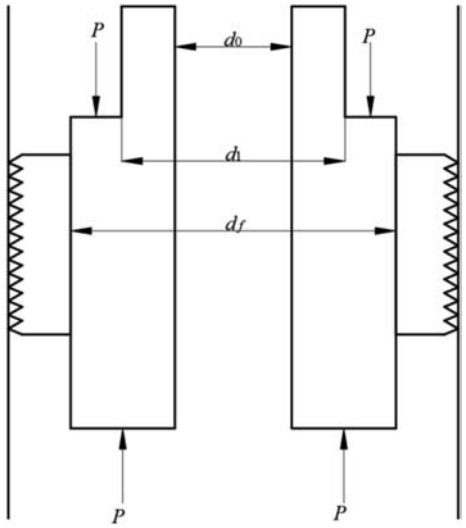


Fig. 31. Packer setting diagram.

diameter of the packer body, mm; d_0 is the inner diameter of the oil tubing, mm; and d_1 is the outer diameter of the tubing, mm.

The outer diameter of the packer body is 140 mm, and the thickener selected is 3½-inch oil tubing of the API specification appropriate to the packer size. The working pressure difference is 260.104 kN, which is less than the load tested in the test, and the slips meet the requirements for downhole use.

6. Conclusion

In this paper, the structural parameters of split-type insert slips are taken as the research object, and the effects of front-end distance, tooth installation space, dip angle of groove, groove depth, and slip wedge angle on the qualitative energy of slip anchors are studied by finite element simulation. An orthogonal test is carried out to optimize the slip structure, and the prototype test verifies the reliability of the research results.

(1) Through the range analysis of the structural parameters of the slip base, it is concluded that the main and secondary effects of the equivalent stress on the slip base are front-end distance, groove depth, tooth installation space, dip angle of groove, and slip wedge angle. The main and secondary effects of casing embedding depth are groove depth, tooth installation space, front-end distance, dip angle of groove, and slip wedge angle. The main and secondary effects on the uniformity of tooth marks are groove depth, tooth installation space, dip angle of groove, front-end distance, and slip wedge angle.

(2) Taking the equivalent stress of the slip base, bite depth, and bite uniformity as the evaluation criteria, the optimal combination of insert slip structural parameters was selected by orthogonal test: front-end distance $L = 12$ mm, tooth installation space $b = 24$ mm, dip angle of groove $\alpha = 76.5°$, groove depth $t = 6.8$ mm, and slip wedge angle $\gamma = 13°$. After the optimization of the structural parameters, the maximum stress of the slip base is reduced by 52.6%, the maximum embedding depth is reduced by 37.9%, and the maximum contact stress is reduced by 30.2%. At the same time, the embedding depth of the casing and the contact stress of the tooth tip are more evenly distributed along the axis. In addition, the slip anchoring effect under the structure is good, and the structural strength is reliable. After setting, it can withstand the axial force of a 152.5-mm casing in the downhole pressure environment of 100 MPa.

CRediT authorship contribution statement

Zhongzhi Hu: Writing – review & editing, Project administration, Conceptualization. **Kaixin Lv:** Writing – original draft, Investigation, Formal analysis, Data curation. **Xiang Gao:** Methodology, Investigation. **Zhilin Ye:** Supervision, Conceptualization. **Tiejun Lin:** Visualization, Supervision.

Declaration of competing interest

The authors declare that they have no competing interests.

Acknowledgements

This work is supported by National Engineering Research Center of Oil & Gas Drilling and Completion Technology Scientific Research Foundation Project (No. NERCDCT202306).

References

Chen, K.P., Shi, X.X., Mi, Y.F., Mi, Y.F., Zhang, H.G., Z, F., 2021. Development and application status and development direction of non-standard oil casing in China. Sci. Technol. Baotou Steel 47 (3), 95–98.

Cui, L.B., Fan, L.Y., Zou, W., 2022. Failure factor analysis and improvement countermeasures of recyclable casing packer in ultra-deep wells in Shunbei oilfield. Well Test. 31 (1), 22–26.

Cui, L., Zou, F., Cheng, J.R., 2023. Sealing characteristics of all-metal soluble bridge plug special-shaped contact structure. Lubr. Eng. 48 (9), 33–40.

Ding, L.L., Lian, Z.H., Chen, S.C., 2011. Numerical simulation of wellbore temperature during high-pressure deep well kills. Oil Drill. Prod. Tech. 33 (4), 15–18.

Deng, C., 2022. Research of Bionic friction-enhanced Surface and Micro-tooth Marks Technology of Packer Slip. Xi'an Shiyou University.

Feng, W.R., Kong, C.Y., Zhang, D.R., 2017. Setting process numerical analysis of inserted tooth slip of sidetracking packer based on plough effect. J. Mach. Des. 34 (6), 55–59.

Hua, Q., Qing, Y.B., 2018. Analysis of common causes of seal failure of high-temperature and high-pressure completion packers. Petrochem. Ind. Technol. 25 (10), 202.

Han, C.J., Peng, X.F., Li, L.T., 2020. Anchoring mechanical behavior of packer slips and its HTHP experimental analysis. Nat. Gas. Ind. 40 (7), 76–82.

Hao, D.L., He, X., Wang, G.R., 2019. Structure optimization of integral slip groove. Chin. J. Eng. Design 26 (5), 534–543.

Lu, X.Q., Zhong, S.M., Li, J., 2011. Design,Development and application of TP140V extra-high strength oil casing for extra-deep complex well service. Kang Kuan 40 (5), 26–30.

Lu, J.K., Guan, Z.R., Luo, F.S., 2022. The analysis of the soluble bridge plug inserted slip base. Mechan. Elect. Eng. Technol. 51 (3), 122–126.

Liu, X.H., 2023. Optimization of inserted tooth slip for high temperature packer based on orthogonal test. China Petrol. Mach. 51 (7), 96–103.

Pang, L., Liu, G.C., Lu, J.P., 2015. The experiments for mechanical properties of 20Cr2Ni4 steel and the coefficient definition of constitutive equation. IOP Conf. Ser. Mater. Sci. Eng. 103 (1), 012028.

Su, Y.N., Lu, B.P., Liu, Y.S., 2020. Status and research suggestions on the drilling and completion technologies for onshore deep and ultra deep wells in China. Oil Drill Prod Tech. 42 (5), 527–542.

Sun, J.S., Liu, W., Wang, Q., 2024. Challenges and development prospects of oil and gas drilling and completion in myriametric deep Formation in China. Drill. Prod. Tech. 47 (2), 1–9.

She, C.Y., 2024. Progress in ultra-deep drilling and completion technology in the Sichuan Basin and its implications for extra-deep wells of more than ten thousand meters in depth. Nat. Gas. Ind. 44 (1), 40–48.

Tian, K., Wang, Z., Hu, L., 2018. Development of Non-API specification TP140V casing for service in extra-deep complex well. Kang Kuan 47 (1), 13–17.

Wang, Z.M., Wen, Z.X., He, Z.J., 2022. Characteristics and enlightenment of new progress in global oil and gas exploration in recent ten years. China Pet. Explor. 27 (2), 27–37.

Wang, H.G., Zhang, J.W., Huang, H.C., 2024. Inspiration and practice of drilling and completion in 10000-Meter ultra-deep Wells in the Gulf of Mexico. Pet. Drill. Tech 52 (2).

Wang, Q., Kong, C., Tang, R., Feng, W., Li, Y., Yang, M., 2023. Optimum design for inserted tooth slips setting process based on the furrow effect. Processes 2023.

Wang, Z.J., Deng, W.D., Lin, Z.C., 2013. Finite element analysis and structure improvements of packer slip in horizontal wells. Oil Drill. Prod. Tech. 35 (4), 78–81.

Wang, F.M., Zhang, Y., Chen, X.J., 2021. Optimum design and experimental analysis of split slip structure. China Petrol. Mach. 49 (10), 71–77.

Xu, T., 2011. Development trend analysis of advanced products and new materials of cemented Carbide. Cem. Carbide. 28 (6), 395–402.

Yang, D., Dou, Y.H., Xu, A.R., 2008. Causes and countermeasures of acid compression packer loss of high temperature and high pressure deep well. China Petrol. Mach. 36 (9), 129–131.

Yu, B., Zhao, W.B., Lei, L.Q., 2013. Finite element analysis of inserted tooth slips of non-metallic bridge plug and optimization. China Petrol. Mach. 41 (8), 68–70+75.

Zhao, Y.P., Li, H.H., Xie, J., 2016. Analysis of failure factors of casing packer during completion and oil testing and countermeasures. Technol. Supervision Petrol. Ind 32 (4), 52–56.

Zhang, D.R., Chen, Y., Zhou, W., 2016. Structural optimization of the slip of drillable bridge plug. Mach. Design Manuf. 2016 (8), 219–223.